UCRL-CONF-201776

Effect of Initial Conditions on Compressible Rayleigh-Taylor Instability and Transition to Turbulence

A.R. Miles, M.J. Edwards, J.A. Greenough – Lawrence Livermore National Laboratory

Submitted to the Nuclear Explosive Design Physics (NEDPC) Conference

Albuquerque, NM, October 19-24, 0003

January 12, 2004

DISCLAIMER

This work was performed under the auspices of the U. S. Department of Energy by the University of California, Lawrence Livermore National Laboratory under Contract No. W-7405-Eng-48.

UCRL-CONF-201776

Effect of Initial Conditions on Compressible Rayleigh-Taylor Instability and Transition to Turbulence

A. R. Miles[1,2], M. J. Edwards[2], J. A. Greenough[2]

[1]Lawrence Livermore National Laboratory,

[2]University of Maryland at College Park

From a dissertation to be submitted to the Graduate School, University of Maryland, by Aaron Miles in partial fulfillment of the requirements for the Ph.D. Degree in Physics.

Perturbations on an interface driven by a strong blast wave grow in time due to a combination of Rayleigh-Taylor, Richtmyer-Meshkov, and decompression effects. In this paper, we present the first results from a computational study of such a system under drive conditions to be attainable on the National Ignition Facility. Using the multi-physics, AMR, higher order Godunov Eulerian hydrocode, Raptor, we consider the late nonlinear instability evolution for multiple amplitude and phase realizations of a variety of multimode spectral types. We show that compressibility effects preclude the emergence of a regime of self-similar instability growth independent of the initial conditions by allowing for memory of the initial conditions to be retained in the mix-

width at all times. The loss of transverse spectral information is demonstrated, however, along with the existence of a quasi-self-similar regime over short time intervals. The initial conditions are shown to have a strong affect on the time to transition to the quasi-self-similar regime.

I. Introduction

The post-linear evolution of the Rayleigh-Taylor (RT) instability[1,2] remains incompletely understood. This is particularly true for multimode perturbations, which are also the most important for practical applications in inertial confinement fusion (ICF) and astrophysics. There is some evidence from theoretical,[3,4] computational,[5] and experimental[6] work that memory of the initial perturbation spectrum is lost as the interface evolves into a self-similar regime in which the mix width grows in proportion with the dominant transverse scale length. The existence of such a regime has yet to be proven, however, even for the most fundamental case of incompressible fluids in a uniform gravitational field. In addition, many physical systems of interest involve compressible systems undergoing time-varying accelerations, where results obtained for the idealized case do not necessarily apply. One class of such systems includes core-collapse supernovae, in which strong blast waves propagate from near the star's core up through layers of progressively less dense material.[7,8] Each driven interface is susceptible to both RT and Richtmyer-Meshkov[9,10] (RM) instabilities.[11] In addition, perturbation

growth results from material expansion in the large-scale velocity gradient behind the shock front.[12,13] Understanding the growth of the resulting turbulent mixing zone may be required to explain the anomalously-fast transport of core material to the star's surface.[7,8,14,15]

Figure 1: Blast-wave pressure, density, and velocity profiles

In order to study this problem, a series of laser-driven laboratory experiments have been designed and conducted on the Nova[16] and Omega[17] lasers,[12,13,18-25] and additional experiments are currently being planned for the National Ignition Facility[26] (NIF). These experiments are intended in part to study the effect of the initial conditions on the nonlinear instability growth, the time to transition, and growth of the post-transition turbulent mixing zone for high Mach number blast-wave driven systems. In this paper, we present computational results for a planer blast-wave-driven system under NIF-like drive conditions. Using the multi-physics, AMR, higher order Godunov Eulerian hydrocode, Raptor,[27] we consider the late nonlinear instability evolution for multiple amplitude and phase realizations of a variety of multimode spectral types. We show that compressibility leads to a breaking of the self-similarity and allows for memory of the initial conditions to be retained in the mix-width at all times. The loss of transverse spectral information is demonstrated, however, along with the existence of a quasi-self-similar regime over short time intervals. The initial conditions are shown to have a strong affect on the time to transition to the quasi-self-similar regime.

II. Code and calculation setup

The simulations are performed using the multi-physics radiation hydrodynamics code Raptor, which uses a 2nd order (in space and time) Godunov method applied to the Euler equations.[27] Raptor is parallelized and uses adaptive mesh refinement (AMR), making it well-suited to problems such as ours that require high resolution in only a portion of the computational domain. We use the LEOS equation of state (EOS) tables and include in the calculations electron conduction but not radiation.[28]

Our hypothetical target (see schematic in Fig. 2a) represents an extension of previous and ongoing decelerating Rayleigh-Taylor experiments performed on the Omega laser and discussed in detail elsewhere.[25] The cylindrical target consists of a 150 μm plastic pusher section (density 1.42 g/cc) in contact with a less dense 2.2 mm payload section. An initial perturbation is machined onto the contact-surface end of the pusher. In place of the carbon foam payload used in the Omega experiments, we assume cryogenic hydrogen with density 0.86 g/cc. We expect that this change, which is motivated by uncertainties in the foam EOS tables,[13] would not qualitatively change the results if carbon foam was to be used in the actual experiments.

The width the computational domain was typically 200 μm, so that the 50 μm wavelength in the previous 2D single-mode experiments corresponds to mode 4. Open boundary conditions are used in the parallel (to the shock) direction while periodic conditions are specified in the transverse direction.

The end of the payload opposite the perturbation is driven with a 1 ns laser pulse, which launches a strong blast wave into the target. We assume a pulse energy of 25 kJ for the NIF-like drive, which is five times greater than that used in the Omega experiments. This higher laser intensity would provide significant drive over a longer period of time than that achieved on previous experiments, and would allow for the generation of larger transverse scales. This is important in part because bubble-merger pictures of multimode instability evolution are generally thought to require multiple merger generations above the largest significant scales present in the initial conditions before a stationary scale-invariant bubble distribution is attained.[5]

The simulations are initiated with a high-velocity, heated, compressed slab with characteristics taken from a laser-driven Lasnex[28] simulation at the end of the laser pulse.

The initial Mach number of the incident blast wave is about 25, corresponding to an initial interface speed of over 130 μm/ns (see Fig. 2a). This is nearly twice the maximum interface speed obtained in the Omega experiments,[13] and the instability is seen to develop about twice as fast. The post-shock Atwood number remains nearly constant at about 0.7. The perturbation growth is dominated by RM for about the first ns, while combined RT and decompression dominate at later times as the interface decelerates in the rarefaction behind the shock front. The simulations are continued out to a maximum of 40 ns, which is about the latest time usable data has been obtained from the Omega experiments.

In order to investigate the dependence of the instability growth to the initial conditions, four different spectral shapes were considered. In a typical case, random phases were assigned to each mode and randomized amplitudes were selected from the

given spectrum. For example, a flat spectrum included modes 4 to 80 with random phases and amplitudes chosen from a uniform distribution. After the amplitude assignment, the resulting spectrum is normalized to give the desired rms amplitude – typically either about 2.5 μm (large ampitude case) or 0.25 μm (small amplitude case). The other three spectral types include a short wavelength component either with or without a single large amplitude long wavelength mode (mode 4) in order to investigate the effect of short wavelength noise on a long wavelength primary mode. The short wavelength component, which includes modes 20 to 80, is given by either e a narrow gaussian centered at mode 40, a broad gaussian centered at mode 40, or a hyperbolic (1/k) spectrum. Multiple realizations were generated from each spectral type in order to provide information about the typical level of fluctuations of measurable quantities within each spectrum.

Figure 3. initial spectra and profiles

III. Results and discussion

Mix width history plots from 52 2D simulations are shown in Fig. 4. Most of the various trajectories fall in to one or the other of two families. The upper family contains the runs with the large amplitude (2.5 μm) mode 4 in the initial spectrum with or without a short wavelength small amplitude component. The short wavelength component is defined by the narrow gaussian, broad gaussian, or hyperbolic spectrum, or by a single mode 40. The rms amplitude in each case differs from the mode 4 amplitude by less than

1%. The lower family consists primarily of runs with the small amplitude short wavelength component with rms amplitude within 50% of 0.25 μm (the average deviation is less than 5%). The small amplitude flat spectrum cases are also contained within the lower family. The large amplitude flat spectrum cases initially lie slightly above the upper family, but then fall below it at about 2-3 ns, eventually joining the lower family between 10 and 20 ns. The two curves below the lower family are from runs with rms amplitude of 0.025 μm (upper curve) and 0.0025 μm (lower curve).

Within the lower family, the amplitude is not well correlated with the initial rms amplitude. Furthermore, the difference between runs with different spectral shape (but with the same order of magnitude initial rms amplitude) is generally not much greater than the difference seen between different amplitude and phase realizations of the same spectrum.

The main point is plotting all the amplitude trajectories together on one plot is to show that they generally diverge in time rather than converging as one might expect during approach to a stationary self-similar bubble distribution. That is, there is no apparent approach to a self-similar regime independent of the initial conditions. This is true even if one considers only those runs from the lower family with only the short wavelength component and with initial rms amplitude of about 0.25 μm. If one assumes self-similarity (ie that the characteristic transverse scale is a constant fraction of the mix-width) and takes into account the time-dependence of the acceleration and the large-scale velocity gradient present in the zero-order hydro, then the spike and bubble growth in each run can be characterized by a constant factor α (the α of $h(t) = \alpha A g t^2$ models). In a true self-similar regime, the value of this parameter should be a universal constant with

weak (if any) dependence on Atwood number.[30] Within the $a_{rms} = 0.25$ μm, shorts only subgroup, we instead find that α_{bubble} varies over a range of about 0.035-0.065 while α_{spike} varies over 0.050-0.100. This nearly covers the entire range of values reported from different experiments and simulations (see, for example, Ref. 31 and references therein), though it falls somewhat short of the values reported for spike growth at this Atwood number (as high as 0.120). Thus the assumption of self-similarity does not lead to a useful means of characterizing the instability growth. Instead, memory of the initial conditions is retained throughout the experiment at least in the mix width. Because of decompression and drive decay, the asymptotic bubble and spike velocities depend on the amplitude and time as well as on the transverse scale and the degree of mix in the layer. The amplitude dependence arises because of the large-scale velocity gradient, proportional to $\Delta r/t$, characteristic of a rarefaction fan. Here Δr is the distance in the parallel direction between any two points, in particular the distance from the unperturbed interface to the position of the spike or bubble tip.

Figure 4. Amplitude histories

However, there is apparently some loss of transverse spectral information and a period of "quasi-self-similar" growth. This is illustrated in two ways Fig. 5. Figure 5a shows a time series of log density plots from a small initial amplitude simulation with a flat spectrum (modes 4-80). During this period, which covers the first 10 ns of growth, the inverse cascade to progressively larger scales is apparent. In Fig. 5b, the images are rescaled so that the mix-width appears approximately constant in time. The similarity in

interface structure in the rescaled images shows that the ratio of dominant transverse scale to mix width does not change much over this time interval. Since the value of this ratio does tend to slowly decrease over time as the material decompresses, we refer to this as a "quasi-self-similar" regime.

The loss of transverse spectral information is illustrated in Fig. 5c, which shows log density plots from simulations with different initial spectral types at early and intermediate times (2.4 and 11.5 ns). Early on, the interface structure is clearly correlated with the initial conditions. In particular. mode 40 is apparent in the early-time narrow gaussian image. The later-time images, on the other hand, appear far more similar to one other. As was noted previously, there is a wide spread in the late time amplitude growth, but the dependence on spectral type within that spread is generally not much larger than the variation between different realizations with the same spectral shape.

A more thorough statistical analysis will be required to give an appropriate description of the quasi-self-similar regime. That analysis, which is currently underway, will be presented in a later paper.

Figure 5. QSSR

The degree of "mixedness", which Youngs calls the molecular mix fraction,[30] provides a good measure of when the transition to the quasi-self-similar regime takes place. The mixedness is defined by

$$\Theta \equiv \frac{\int \langle f(1-f) \rangle dz}{\int \langle f \rangle dz \int \langle 1-f \rangle dz}$$

where f is the volume fraction of either of the two fluids, the averaging is done in the transverse direction, and the integral is performed in the parallel direction through the extent of the mix region. The time histories of the mixedness from all 52 2D simulations are shown in Figure 6. Again, most of the curves fall into one of two families. The upper family contains runs without the large amplitude mode 4, while the lower family consists of all the runs with the large mode 4. In both cases, there is a clear transition to a from a state that is not well-mixed to a state with higher degree of mixedness that tends to an asymptotic value between about 0.6 and 0.8. With no large mode 4, this transition occurs within a few ns, and corresponds to the transition to the quasi-self-similar regime. The same transition occurs when the large mode 4 is included in the initial spectrum, but the time to transition is several times longer. Thus the presence of the long wavelength mode delays the transition to a turbulent-like state. Comparison of Fig. 6 with amplitude history plots shows that, in addition to the increase in mixedness, transition to the quasi-self-similar regime is marked by a decrease in the spike velocity and often an increase in the bubble velocity. The spike velocity decreases in particular for the runs with large-amplitude mode 4, where the transition is associated with the breakup of the primary spikes. This breakup allows the spikes' parallel energy to be diverted into the transverse direction and results in a decrease in the effective Atwood number in the mix region. When the initial spectrum gives an array of nearly identical bubbles, transition can allow for bubble competition and the generation of larger scales, resulting in an increase in the velocity of the bubble front.

In a true self-similar regime (at least for the case of incompressible flow, no RM component, and constant acceleration – all of which are violated here), the post-transition mixedness should be a universal constant depending only on the Atwood number. For a density ratio similar to ours (and with very weak density ratio dependence), Youngs reports a value of about 0.83 in 3D and 0.54 in 2D.[32] The values we find are distributed throughout this range, and are consistently higher than the reported 2D value.

Finally, we note that there is no observed turbulent mixing transition[33] in the simulations. This is to be expected due to the low effective Reynolds number and the 2D nature of the simulations.

In general, the evolution can be divided into three phases, as shown in Figure 7. During the early time phase (Phase I - which actually included the linear early nonlinear, and into the nonlinear regimes), the growth rate is determined by the most unstable mode. RM dominates initially, but only for about 1 ns. During this period, the inverse cascade to larger scales is initiated, and there are up to three generations of bubble merger. The growth rate depends on the rms amplitude, but does not depend strongly on the spectral details. During Phase II, there are changes in the growth rates (sometimes rather abrupt) that result in a strong dependence on the spectral details as well as the initial rms amplitude. Consideration of separate spike and bubble amplitude histories shows that the spike growth is more sensitive than the bubble growth to the initial spectrum. Phase III begins when mode 1 emerges as the dominant transverse scale after up to five bubble merger generations. After this scale is reached, the growth is single-mode-like rather than self-similar-like. One would tend to conclude at this point that this signals the end of the calculation's range of validity because the computational box has been "filled" so that

end effects corrupt further evolution. In fact, calculations run with twice or even four times the nominal box size generally show no significant change in the perturbation growth history and or the late-time dominant transverse scale. We attribute this to the decaying nature of the driving acceleration. As the acceleration approaches zero, the time to generate larger scales (which even with constant acceleration take longer to form than shorter scales) tends to infinity. Thus the decaying acceleration profile coupled with the finite experiment duration introduces an "effective box size" even in the absence of an experimentally or computationally-imposed physical box size.

IV. Conclusions and future directions

We have presented preliminary results from 52 2D simulations of hydrodynamically-unstable interfaces driven by a strong blast wave under NIF-like drive conditions. The mix-width time histories show no apparent approach to a self-similar regime independent of the initial conditions. This is due to decompression and drive decay, which result in an asymptotic velocity that depends on the amplitude and time as well as on the transverse scale and the degree of mix in the layer. For sufficiently long but finite experiment duration, drive decay also leads to an effective box size that sets a maximum transverse scale that can be generated. After this scale is reached, the growth is single-mode-like rather than self-similar-like. There is, however, a period of quasi-self-similar growth after generation of scales larger than the initial conditions but before the generation of the effective-box-size scale. Transition to the quasi-self-similar regime is

marked by an increase in the degree of mixedness, a decrease in the spike velocity, and often an increase in the bubble velocity.

Analysis of turbulent spectral evolution, necessary to properly describe the quasi-self-similar regime, is currently underway and will be presented in a later paper. We are also beginning 3D calculations to investigate the dimensionality dependence, and are working to formulate a statistical-mechanical interface evolution model to include the effects of decompression and drive decay as well as some accounting for the RM contribution.

V. Acknowledgements

This work was performed under the auspices of the U. S. Department of Energy by the University of California, Lawrence Livermore National Laboratory under contract No. W-7405-Eng-48.

VI. References

[1]J. W. S. Rayleigh, *Scientific Papers* (University press, Cambridge, 1899).

[2]G. I. Taylor, Proc. R. Soc. London, Ser. A **201**, 192 (1950).

[3]J. Glimm, D. H. Sharp, Phys. Rev. Lett. **64**(18), 2137 (1990).

[4]U. Alon, J. Hecht, D. Mulamel, and D. Shvarts, Phys. Rev. Lett. **72**(18), 2867 (1994).

[5]D. L. Youngs, Physica D **12**, 32 (1984).

[6]K. I. Read, Physica D **12**, 45 (1984).

[7]W. D. Arnett, J. N. Bachall, R. P. Kirshner, and S. E. Woosley, Ann. Rev. Astron. Astrophys. **27**, 629 (1989).

[8]W. Hillebrandt and P. Hoflich, Rep. Prog. Phys. **52**, 1421 (1989).

[9]R. D. Richtmyer, Commun. Pure Appl. Math. **13**, 297 (1960).

[10]E. E. Meshkov, *Izv*. AN SSSR Mekhanika Zhidkosti I Gaza **4**(5), 151 (1969).

[11]R. Chevalier, Ap. J**. 207**, 872 (1976).

[12]J. Kane, D. Arnett, B. A. Remington, S. G. Glendinning, G. Bazan, R. P. Drake, B. A. Fryxell, R. Teyssier, and K. Moore, Phys. Plasmas **6**(5), 2065 (1999).

[13]A. R. Miles, D.G. Braun, M.J. Edwards, H.F. Robey, R.P. Drake, *et al*., "Numerical Simulation of Supernova-Relevant Laser-driven Hydro Experiments on OMEGA", submitted to *Phys. Plasmas*.

[14]D. Arnett, B. Fryxell, E. Muller, Astrophys. J. **341**, L63 (1989); E. Muller, B. Fryxell, D. Arnett, *Astron. Astrophys*. **251**, 505 (1992)

[15]B. A. Remington, J. Kane, R. P. Drake, *et al*., Phys. Plasmas **4**, 1994 (1997).

[16]E. M. Campbell, Las. Part. Beams **9**, 209 (1991).

[17]J. M. Soures, R. L. McCrory, C. P. Verdon, *et al*., Phys. Plasmas **5**, 2108 (1996).

[18]K.S. Budil, B.A. Remington, T.A. Peyser, K.O. Mikaelian, P.L. Miller, *et al*., Phys. Rev. Lett. **76**, 4536 (1996).

[19]J. Kane, D. Arnett, B.A. Remington, S.G. Glendinning, J. Castor, *et al*., Astrophys. J. **478**, L75 (1997).

[20]J. Kane, D. Arnett, B.A. Remington, S.G. Glendinning, R. Wallace, *et al.*, in *Second Oak Ridge Symposium on Atomic and Nuclear Astrophysics*, Oak Ridge, Tenessee, 1998).

[21]J. Kane, D. Arnett, B.A. Remington, S.G. Glendinning, G. Bazan, *et al.*, Astrophys. J. Suppl. **127**, 365 (2000).

[22]J.O. Kane, H.F. Robey, B.A. Remington, R.P. Drake, J. Knauer, *et al.*, Phys. Rev. E **63**, 055401R (2001).

[23]H.F. Robey, J.O. Kane, B.A. Remington, R.P. Drake, O.A. Hurricane, *et al.*, Phys. Plasmas **8**, 2446 (2001).

[24]R.P. Drake, H.F. Robey, O.A. Hurricane, Y. Zhang, B.A. Remington, *et al.*, Astrophys. J. **564**, 896 (2002).

[25]H.F. Robey, Y. Zhou, A.C. Buckingham, P. Keiter, B.A. Remington, *et al.*, Phys. Plasmas **10**, 614 (2003).

[26]S. ome Authors, NIF reference. Possibly JA Paisner, EM Campbell, and WJ Hogan, Fusion Technol**. 26**, 755 (1994).

[27]L. H. Howell and J.A. Greenough, J. Comp. Phys. **184**, 53 (2003).

[28]S. ome Authors, LEOS reference

[29]G. B. Zimmerman and W. L. Kruer, Comments on Plasma Physics and Controlled Fusion **2**, 51 (1975).

[30]D. L. Youngs, Phys. Fluids A **3**(5), 1312 (1991).

[31]G. Dimonte, Phys. Plasmas **7**(6), 2255 (2000).

[32]D. L. Youngs, Las. Part. Beams **12**(4), 725 (1996).

[33]P. E. Dimotakis, J. Fluid Mech. **409**, 69 (2000).

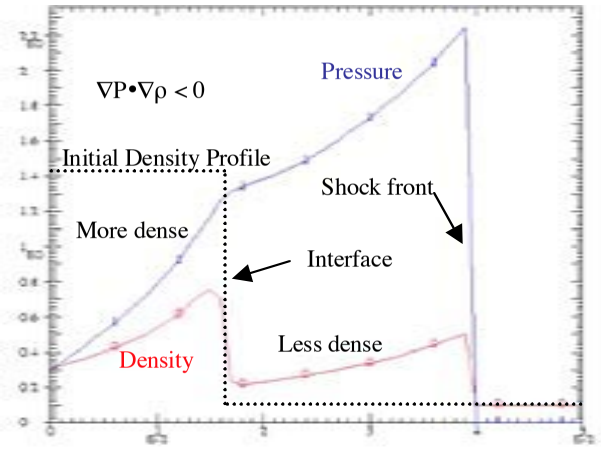

Figure 1: Blast wave refraction through a heavy-light interface. The Rayleigh-Taylor instability criterion is satisfied at the post-shock interface, which is also Richtmyer-Meshkov unstable. The fluid velocity falls off approximately linearly behind the shock front. The corresponding decompression results in additional perturbation growth.

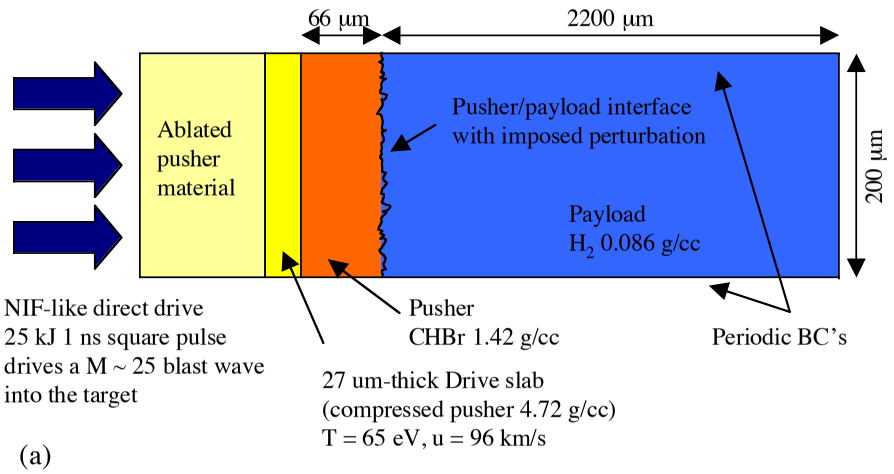

(a)

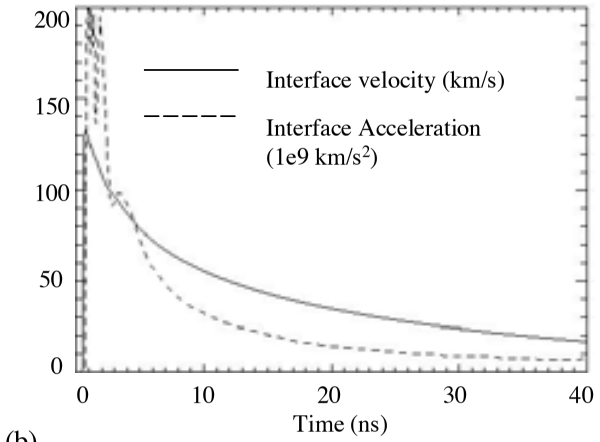

(b)

Figure 2: (a) Target schematic (not to scale). (b) Variation in time of interface velocity and deceleration.

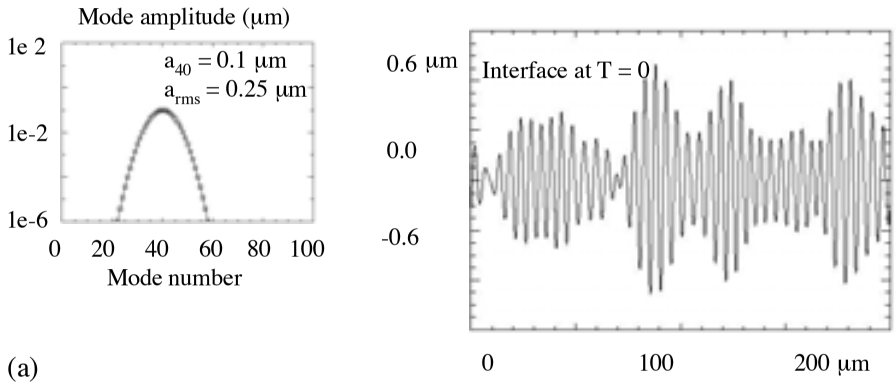

(a)

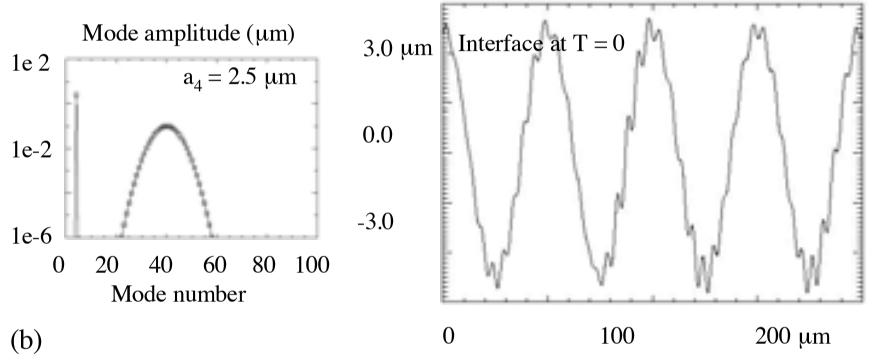

(b)

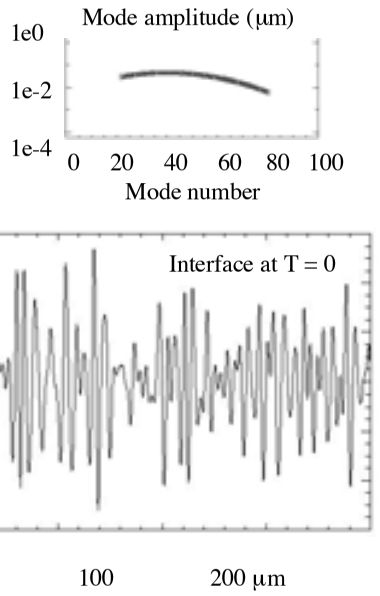

(c)

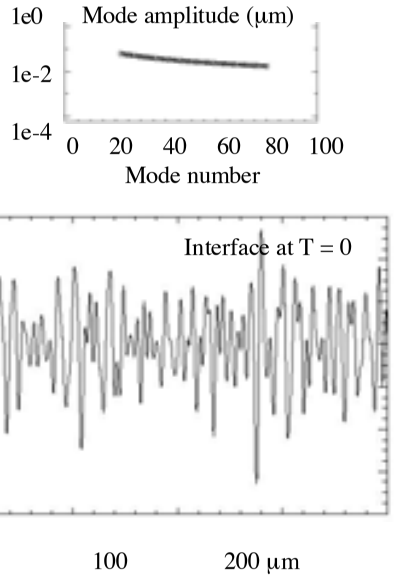

(d)

Figure 3: Initial spectral shapes and typical interface profiles. (a) Narrow gaussian without large-amplitude mode 4. (b) Narrow gaussian with large-amplitude mode 4. (c) Broad gaussian and (d) hyperbolic without large-amplitude mode 4.

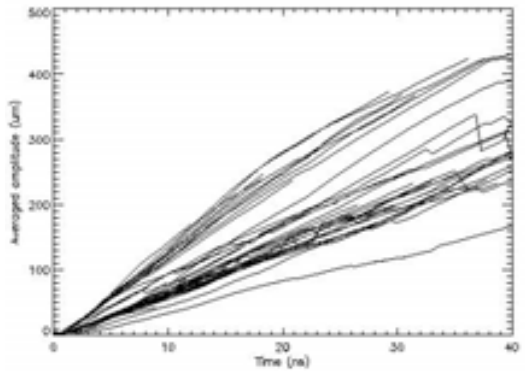

Figure 4: Mix width histories from 52 2D simulations with different spectral initial conditions. There is no apparent approach to a self-similar regime independent of the initial conditions. Even when runs with large mode 4 are excluded, α_b varies over a range of about 0.035-0.065 for different IC's, while α_s varies over about 0.050-0.100.

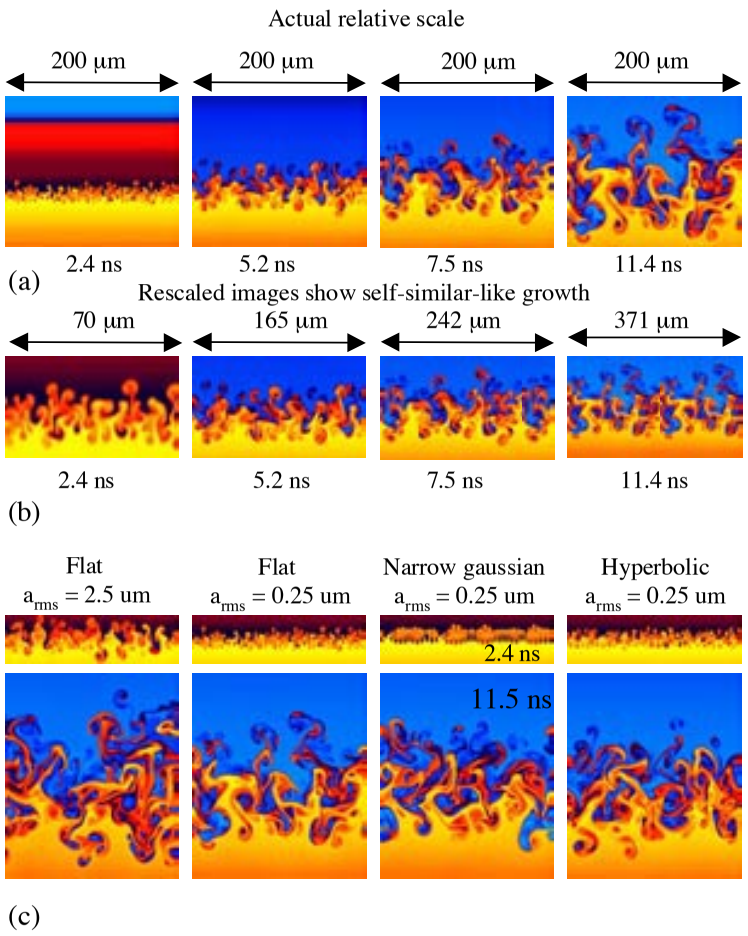

Figure 5: Quasi-self-similar regime. (a) A time series of log density plots from a small initial amplitude simulation with a flat spectrum (modes 4-80) shows the inverse cascade to progressively larger scales. (b) The same images are rescaled so that the mix-width appears approximately constant in time. The similarity in interface structure in the rescaled images shows that the ratio of dominant transverse scale to mix width does not change much over this time interval. (c) The loss of transverse spectral information is illustrated by log density plots from simulations with different initial spectral types at early and intermediate times (2.4 and 11.5 ns). Early on, the interface structure is clearly correlated with the initial conditions. The later-time images appear far more similar to one other.

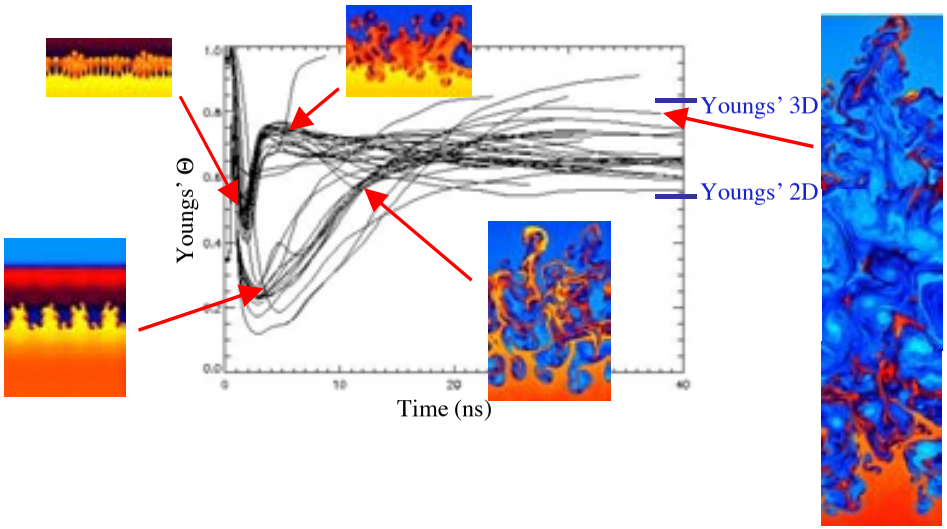

Figure 6: Degree of mixedness for all 52 2D simulations. Transition to "turbulence" (ie onset of quasi-self-similar regime) results in an increase in mixedness. However, there is no observed turbulent mixing transition. For a similar density ratio, Youngs* reports $\Theta \approx 0.83$ in 3D and $\Theta \approx 0.54$ in 2D [D.L. Youngs, Lasers and Particle Beams, 12(4), 725 (1994)].

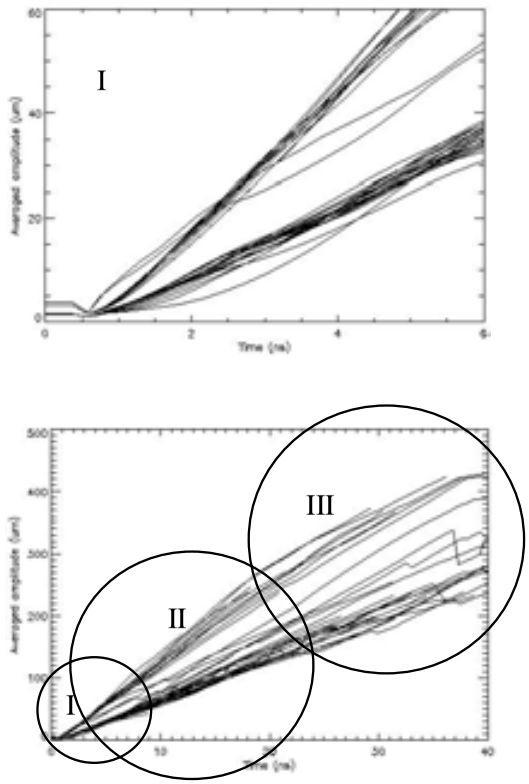

Figure 7: Three phases of instability growth. Phase I: The early-time (linear, early nonlinear, and into nonlinear) phase is dominated by RM for about 1 ns. The growth rate is determined by the most unstable mode, and the inverse cascade is initiated. Phase II: Changes in growth rate result in strong dependence on spectral details in addition to the initial a_{rms}. Phase III: Mode 1 emerges as the dominant transverse scale after up to 5 bubble merger generations. The acceleration profile introduces an "effective box size". The asymptotic velocity depends on amplitude, time in addition to the transverse scale and the degree of mix in the layer.

University of California
Lawrence Livermore National Laboratory
Technical Information Department
Livermore, CA 94551